Journal of the Korean Physical Society, Vol. 77, No. 8, October 2020, pp. 653∼661

Flatness Measurement of a Mosaic Focal Plane by using a Coaxial Multispectral Laser

Chang-hua Liu* and Ning-Xin Guo
Changchun Institute of Optics, Fine Mechanics and Physics, Chinese Academy of Sciences , Changchun 130033, China and University of Chinese Academy of Sciences, Beijing 100049, China

Jian-Li Wang, Tao Chen and Zhi-Yong Wu
Changchun Institute of Optics, Fine Mechanics and Physics, Chinese Academy of Sciences, Changchun 130033, China

Xue Cheng
Suzhou Institute of Biomedical Engineering and Technology, Chinese Academy of Sciences, Suzhou 215163, China

(Received 16 March 2020; revised 7 May 2020; accepted 3 June 2020)

The wide-field telescope will be an important tool in the discovery and birth of new theories of astronomy in future. The detectors in this kind of telescope mostly adopt a mosaic focal plane array. The focal depth of a large-F-number optical system is very small, and the flatness of the mosaic detector should be less than half the focal depth. In this paper, a new flatness measurement and data processing method is developed. A flatness measurement platform composed of a high-precision gantry platform and a coaxial multispectral displacement meter was built. The flatness of a single detector was measured under uncooled and cooled working conditions, and data processing was conducted, in which the root mean square (RMS) and the peak–valley (PV) values of the cooled detector were 0.0017 mm and 0.0112 mm, respectively. Next, a 2 × 6 mosaic model of the focal plane with a dimension of 148.5 mm × 168.5 mm was built using a metal detector model. The measurement platform was used to measure the flatness of the mosaic focal plane. According to the measurement results, the preliminary installation and mosaic adjustment were completed. The final RMS and PV values of the mosaic focal plane are 0.009 mm and 0.0808 mm, respectively. The experimental results show that the measurement and the data processing method can accurately reflect surface information on the detectors. This suggests that the method has great potential for use in ensuring the accuracy of wide-field telescope equipment in all applicable research areas.

Keywords: Focal plane, Flatness, Detector array, Laser gauge
DOI: 10.3938/jkps.77.653

I. INTRODUCTION

In the application of the modern digital sky survey with wide-field telescopes, the flatness of the detector is an important characteristic, especially for mosaic detectors. The mosaic focal plane is composed of several detectors, which are coplanar after precise alignment. Shown in the Fig. 1 is the hyper suprime-cam (HSC) of Japan's Subaru Telescope. In the development process, the flatness of the detector needs to be measured many times at different stages and under different working conditions to ensure that the flatness of the detector meets the requirement of half the focal depth of the system. Generally, the surface of the detector is coated with an antireflection film and the reflectivity is only 1% to 4%. The detectors are sensitive optical elements, which can only be measured using a non-contact method, and the measurement of cooled detectors in dewar needs to be performed through the window. Choosing an appropriate method of carrying out measurements for single-detector mosaic detectors is very complicated. At present, many wide-field telescopes have a corresponding measurement platform set up: for example, the large synoptic survey telescope (LSST) adopted a Keyence LT-9030M triangle laser head to form a measurement platform for the mosaic camera [1]; the korea microlensing telescope net-work (KMTNet) adopted a SmartScope Vantage 300 of optical gaging produts (OGP) from America to realize composite mea-

*E-mail: changhua-liu@163.com

 ©2020 The Korean Physical Society

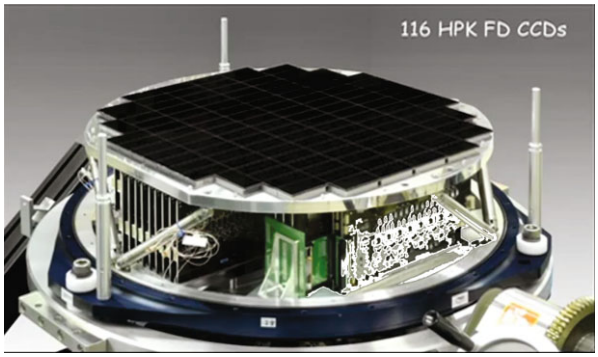

Fig. 1. Subaru hyper suprime-cam (HSC).

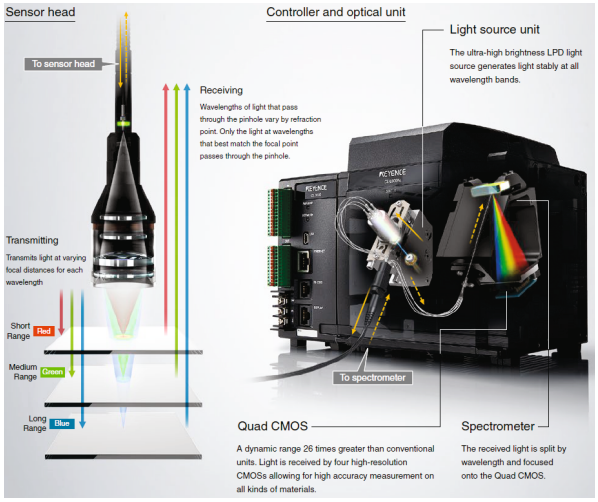

Fig. 2. Composition diagram of the Keyence CL-3000.

surement for the 2 × 2 mosaic charge coupled devices (CCDs) [2]; the HSC of the Subaru telescope adopted a Mitaka-Koki NH3-SP high-precision measurement system [3]; a Keyence LK-H082 triangular laser measuring head from Japan is used by the european southern observatory (ESO) to form the measurement system, which has been successfully applied to the measurement of the curved detector and the Omega-Cam mosaic camera; and the Image Based Measurements method is used for dark energy camera (DECam) to perform the measurements of the detectors [4]. This study aims to develop a new method of flatness measurement and data processing by using a flatness measurement platform composed of a high-precision gantry platform and a coaxial multispectral displacement meter.

II. METROLOGY PRINCIPLE

1. Metrology Requirements

The surface of the detector is a thin silicon wafer coated with an anti-reflection film, which can convert

Fig. 3. Advantages of a coaxial color laser measurement.

photons into electronic signals for imaging. In general, detectors are placed in a vacuum dewar with a window. The following requirements must be met to measure the surface geometry of the detectors:

a) non-contact measurement method;
b) suitable for low-reflectivity coated surface measurement;
c) measurement can be made through the window;
d) the measurement accuracy should be submicron level.

2. Metrology Principle

The Keyence CL-3000 series of displacement meters from Japan has adopted a brand-new design in which the measuring probe and processing unit are independent; the measuring probe only has a group of optical lenses, and the light source adopted is an ultra-high-brightness color laser. Light of different wavelengths is focused at a range of different focal lengths, and the light reflected by the measured object is filtered through the pinhole. Only the light that most conforms to the focal wavelength can pass through the pinhole. The processing unit decomposes the light received into four high-resolution complementary metal oxide semiconductor (CMOS) sensors according to wavelength and realizes high-precision measurement of displacement. This method of measurement is called the dispersion confocal principle. The composition diagram of the CL-3000 is shown in Fig. 2.

3. Advantages

Compared with the traditional triangular laser measurement, the advantages of the new measurement, which are illustrated in Fig. 3, are as follows [5]:

a) the principle of color confocal measurement is adopted to achieve a wide range of high-precision measurements;
b) the heating element is designed separately from the measuring probe, and the influence of heating and electrical interference is zero;
c) the glass refraction deviation can be compensated for, and the focal plane can be measured through the window.

Fig. 4. Gantry for the flatness measurement.

Fig. 5. Control software interface.

III. DESIGN OF THE MEASUREMENT PLATFORM

The Keyence's displacement meter measures distance information. It needs to coordinate with a two-dimensional motion platform to measure the height of the array points on the surface of the object to be measured. A point cloud is used to reconstruct the detector surface to obtain the flatness of a single detector and mosaic array detectors. Therefore, we constructed an experimental platform for the measurement of detector surface information.

The function of the measurement platform is to drive the laser displacement meter to carry out two-dimensional motion in a plane and to obtain the distance between the measured object and the measuring head. The measuring accuracy is better than 1 μm. For the measurement of the mosaic accuracy of the detectors, the travel range of the platform's two-dimensional motion is designed to be 550 mm × 550 mm. After several forms of measurement platforms had been compared, a gantry, which has good stability, high measurement accuracy, large bearing capacity, and expansibility, as shown in Fig. 4, was chosen for the measurement.

Table 1. Parameters of the platform.

Performance Indicators	Value
Range of motion (mm)	550 × 550
Repeat positioning accuracy (μm)	±1
Range of measurement (mm)	±3.7
Accuracy (μm) at ±1mm	±0.72
Spot diameter (μm)	500
Acceleration (g)	1
Maximum speed (mm/s)	0.5

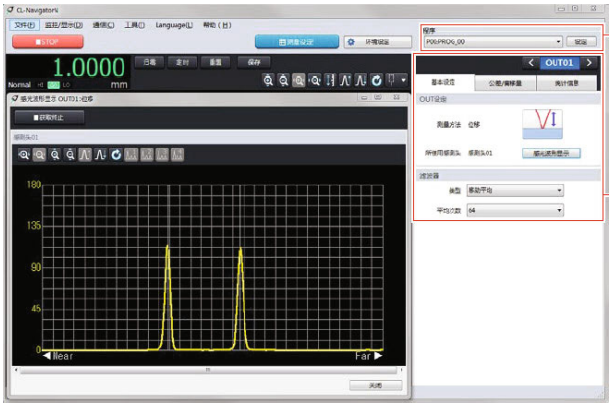

Fig. 6. Measurement setting interface.

As its base, the measurement platform uses marble, which can better ensure the accuracy and the stability of the detector flatness measurement. After manual grinding, the marble platform can obtain an extremely high-precision guide rail installation interface and cooperate with a THK high-precision ball linear track from Japan to obtain high-precision linear motion. The gantry platform is driven by three groups of linear motors, for which the longitudinal axis is driven by two master–slave linear motors. The linear motor is a non-contact direct drive mode, which does not interfere with the platform's movement. The measurement platform uses an ACS multi-axis drive controller from Israel and coordinates with the high-precision grating scale feedback signal to compensate for the two-dimensional motion error of the platform, finally ensuring that the accuracy requirements of the detector flatness measurement are met. Table 1 shows the main performance parameters of the platform.

The platform has its own coordinate system, and the origin of the coordinates is located at the center of the two-dimensional motion. During the measurement, firstly, control software is used as shown in Fig. 5 to initialize the platform; the detector to be measured is placed under the probe such that its focal spot falls on one corner of the detector, and the distance between the detector and the laser displacement meter is adjusted

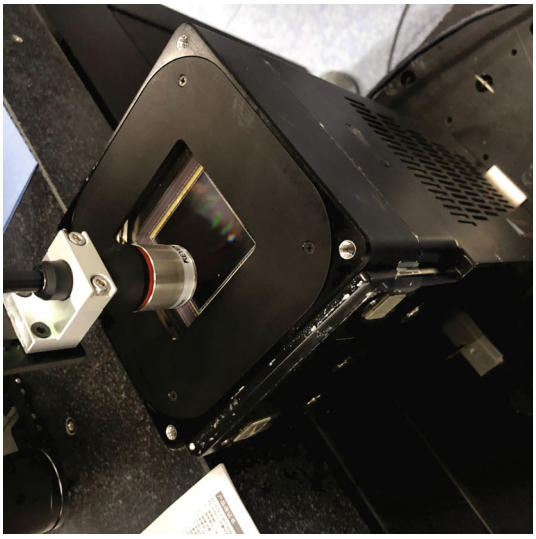

Fig. 7. Flatness measurement of a single detector.

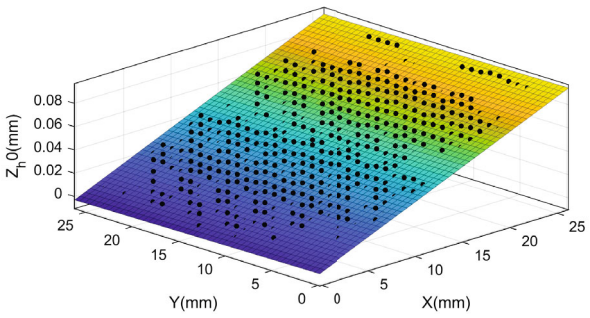

Fig. 8. Fitting plane of the point cloud.

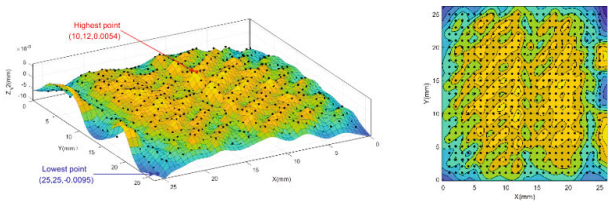

(a) Fitting surface (b) Contour map

Fig. 9. Information on the surface of the uncooled detector.

to approach zero. Secondly, the laser measuring head is moved in one direction of the gantry to the adjacent corner of the detector, the orientation of the detector is adjusted, and the direction of motion is either horizontal or vertical to the detector. Before the formal measurement, the measurement parameters of the laser displacement meter, including measurement type (reflection measurement or transmission measurement), sampling frequency, measurement correction, and data storage, as shown in Fig. 6, depicting the setting interface of the laser displacement meter, need to be set.

IV. FLATNESS OF A SINGLE DETECTOR

The flatness of a Princeton Instruments Quad-RO 4320 camera from America was measured under both cooled and uncooled working conditions (at −30 °C) by using the gantry, as shown in Fig. 7. Taking the upper left corner of the detector as the coordinate origin, with an interval of 1 mm measured, the height information of 25 × 25 array points on the surface; the point cloud information of the detector surface was obtained, and MATLAB was used for data processing.

1. Flatness Measurement of an Uncooled Detector

The uncooled detector's flatness information Z_h0 was measured. The height information of the detector array points is shown in Table 2. A relative tilt exists between the measured surface and the measurement platform [6, 7]. First, the fitting plane of the point cloud needs to be calculated before the relative distance between the initial data and the fitting plane is calculated. The fitting plane of the detector is as shown in Fig. 8, the R^2 of the fitting plane is 0.991, and the adjusted R^2 is 0.9909. The equation of the fitting plane from the array point is

$$Z\_h1 = 0.0007686 + 0.003572 \cdot X - 0.0001103 \cdot Y \quad (1)$$

The deviation between the collection point and the fitting plane is

$$Z\_h2 = Z\_h0 - Z\_h1 \quad (2)$$

After re-fitting the revised data, we obtain the fitting surface and contour map, as shown in Fig. 9. This figure shown that the flatness of the detector is good, especially the relative deviation of the central part of the detector, which is less than 5 μm, although a obvious collapse at the four corners of the detector. After calculation, the root mean square (RMS) value of the uncooled detector is 0.0025 mm, and the peak-valley (PV) value is 0.0149 mm. The highest and the lowest points appear at (10, 12, 0.0054) and (25, 25, −0.0095), respectively.

2. Flatness Measurement of a Cooled Detector

The flatness of the detector will change after being cooled, so the flatness of the cooled detector should be measured next to evaluate the effect of temperature on the detector flatness. The temperature of the cooled detector was −30 °C, and the height information Z_e0 of the array point of the cooled detector is shown in Table 3. A relative tilt exists between the measured surface and the measurement platform. First, the fitting plane of the point cloud needs to be calculated before the relative

Table 2. Height of the uncooled detector.

X/Y(mm)	1	2	3	4	5	6	7	8	9	10	11	12	13
1	−0.0026	0.0026	0.0084	0.01	0.0138	0.0195	0.0256	0.0284	0.0312	0.0353	0.0399	0.0435	0.0435
2	0.0008	0.0033	0.0074	0.0146	0.0146	0.0212	0.0246	0.0307	0.0328	0.0358	0.0399	0.0458	0.0456
3	0.0003	0.0061	0.0067	0.0125	0.0179	0.0238	0.0238	0.0287	0.0348	0.0387	0.0384	0.0445	0.0445
4	−0.001	0.0046	0.009	0.0095	0.0159	0.0228	0.0256	0.0276	0.0315	0.0369	0.0399	0.043	0.043
5	0.0008	0.0031	0.01	0.0133	0.0141	0.021	0.0266	0.032	0.031	0.0353	0.041	0.0471	0.0471
6	0.0026	0.0049	0.0084	0.0154	0.0174	0.022	0.0253	0.0315	0.0353	0.0366	0.0402	0.0466	0.0466
7	0.0015	0.0074	0.0084	0.0143	0.0189	0.0251	0.0248	0.0284	0.0351	0.0392	0.0399	0.0443	0.0443
8	0.001	0.0054	0.01	0.0118	0.0187	0.0233	0.0264	0.0294	0.0315	0.0376	0.041	0.0456	0.0453
9	0.0013	0.0033	0.0113	0.0136	0.0159	0.0207	0.0276	0.0315	0.0325	0.0351	0.043	0.0466	0.0466
10	0.0026	0.0061	0.01	0.0169	0.0172	0.0233	0.0261	0.0323	0.0351	0.0379	0.0412	0.0479	0.0481
11	0.0015	0.0074	0.0095	0.0154	0.0202	0.0248	0.0256	0.0294	0.0364	0.0392	0.0404	0.0456	0.0456
12	0.0003	0.0067	0.0102	0.0118	0.0182	0.0246	0.0264	0.0292	0.0323	0.0392	0.0412	0.0445	0.0445
13	0	0.0036	0.0113	0.0131	0.0146	0.021	0.0276	0.0315	0.031	0.0353	0.0417	0.0474	0.0471
14	0.0028	0.0046	0.0095	0.0161	0.0172	0.0223	0.0253	0.0317	0.0348	0.0361	0.0397	0.0463	0.0468
15	0.0013	0.0082	0.0087	0.0143	0.0192	0.0256	0.0248	0.0287	0.0348	0.0397	0.0394	0.0451	0.0438
16	−0.0008	0.0059	0.0108	0.0118	0.0179	0.0233	0.0269	0.0289	0.0317	0.0371	0.042	0.0438	0.0438
17	0	0.0023	0.01	0.0125	0.0154	0.0197	0.0259	0.0302	0.0307	0.0333	0.0404	0.0453	0.0453
18	0	0.0049	0.0087	0.0143	0.0161	0.0218	0.0248	0.03	0.033	0.0358	0.0384	0.0451	0.0453
19	−0.0003	0.0064	0.009	0.0143	0.0182	0.0241	0.0246	0.0276	0.034	0.0379	0.0394	0.0428	0.043
20	−0.0015	0.0056	0.0095	0.0115	0.0177	0.0228	0.0253	0.0287	0.032	0.0376	0.0407	0.0438	0.0438
21	−0.0023	0.002	0.009	0.0108	0.0136	0.0195	0.0256	0.0287	0.0297	0.0335	0.0402	0.0443	0.0443
22	0	0.0023	0.0072	0.0133	0.0141	0.0197	0.023	0.0297	0.0317	0.0338	0.0376	0.0445	0.0451
23	−0.0018	0.0049	0.0061	0.0113	0.0169	0.0225	0.0225	0.0269	0.0333	0.0369	0.0374	0.0417	0.042
24	−0.0041	0.0031	0.0072	0.0084	0.0148	0.0218	0.0243	0.0264	0.0297	0.0358	0.0397	0.0412	0.0412
25	−0.0054	0	0.0059	0.0079	0.0102	0.0166	0.0225	0.0271	0.0266	0.0312	0.0371	0.0425	0.0425

X/Y(mm)	14	15	16	17	18	19	20	21	22	23	24	25
1	0.0479	0.0504	0.0548	0.0594	0.0637	0.0666	0.0714	0.0742	0.0748	0.0765	0.0804	0.0845
2	0.0474	0.053	0.0568	0.0607	0.065	0.0694	0.0722	0.0753	0.0771	0.0776	0.0819	0.0865
3	0.0492	0.0522	0.0581	0.0609	0.0658	0.0701	0.073	0.0737	0.0778	0.0783	0.0824	0.0893
4	0.0489	0.0522	0.0563	0.062	0.0645	0.0689	0.0735	0.075	0.0765	0.0794	0.0814	0.0893
5	0.0515	0.053	0.0581	0.0622	0.0678	0.0684	0.0732	0.0771	0.0778	0.0794	0.0842	0.0899
6	0.0504	0.0563	0.0591	0.0622	0.0676	0.0719	0.073	0.0778	0.0796	0.0801	0.0847	0.0919
7	0.0502	0.0543	0.0607	0.0622	0.0663	0.0707	0.0748	0.0776	0.0804	0.0801	0.0835	0.0922
8	0.0517	0.0515	0.0579	0.0625	0.0663	0.0686	0.074	0.0755	0.0788	0.0804	0.0824	0.0904
9	0.0512	0.054	0.0566	0.0617	0.0666	0.0699	0.0737	0.0778	0.0776	0.0799	0.0829	0.0901
10	0.0499	0.055	0.0602	0.0609	0.0671	0.0707	0.075	0.0776	0.0799	0.0794	0.084	0.0899
11	0.0497	0.0538	0.0596	0.0625	0.0666	0.0719	0.0742	0.0758	0.0796	0.0799	0.084	0.0837
12	0.0507	0.0522	0.0571	0.0625	0.0658	0.0696	0.075	0.076	0.0778	0.0794	0.0822	0.0824
13	0.0507	0.053	0.0571	0.062	0.0676	0.0686	0.0735	0.0758	0.0783	0.0788	0.0829	0.0822
14	0.0486	0.0558	0.0586	0.062	0.0673	0.0717	0.0727	0.0771	0.0788	0.0796	0.0842	0.0832
15	0.0499	0.054	0.0607	0.0612	0.0663	0.0709	0.0745	0.0765	0.0806	0.0794	0.0845	0.0835
16	0.0504	0.0512	0.0573	0.0632	0.0655	0.0681	0.0737	0.0753	0.0791	0.0806	0.0819	0.0829
17	0.0504	0.052	0.055	0.0602	0.066	0.0673	0.0712	0.0765	0.0763	0.0786	0.0829	0.0909
18	0.0481	0.054	0.0586	0.0581	0.0653	0.0694	0.0717	0.0755	0.0791	0.0773	0.0827	0.0906
19	0.0471	0.052	0.0586	0.0609	0.063	0.0699	0.073	0.074	0.0783	0.0794	0.0814	0.0904
20	0.0507	0.0494	0.0553	0.0614	0.0653	0.0663	0.0742	0.074	0.076	0.0783	0.0817	0.0906
21	0.0481	0.0509	0.0532	0.0596	0.0648	0.0663	0.0707	0.074	0.075	0.0758	0.0806	0.084
22	0.0456	0.0525	0.0563	0.0576	0.0635	0.0681	0.0696	0.0732	0.076	0.0758	0.0814	0.0817
23	0.0466	0.0507	0.0571	0.0589	0.0627	0.0686	0.0712	0.0709	0.0773	0.0763	0.0806	0.0806
24	0.0476	0.0492	0.0538	0.0604	0.0627	0.0658	0.0722	0.0719	0.075	0.0771	0.0788	0.0794
25	0.0466	0.0481	0.0522	0.0571	0.0632	0.063	0.0678	0.0712	0.0735	0.0745	0.0791	0.0778

Table 3. Height of the cooled detector.

X/Y(mm)	1	2	3	4	5	6	7	8	9	10	11	12	13
1	0.0914	0.0932	0.0957	0.0993	0.0993	0.1057	0.1085	0.1126	0.1155	0.1221	0.1244	0.1288	0.1321
2	0.0904	0.0929	0.0937	0.0993	0.0993	0.1024	0.1103	0.1111	0.1139	0.1213	0.1242	0.1265	0.1303
3	0.0904	0.0891	0.0942	0.0957	0.0957	0.1042	0.1062	0.1098	0.1132	0.1198	0.1226	0.1234	0.1277
4	0.0891	0.0906	0.0932	0.097	0.097	0.1011	0.1075	0.1098	0.1103	0.1185	0.1219	0.1262	0.1288
5	0.0878	0.0876	0.0901	0.0945	0.0945	0.1039	0.1039	0.1078	0.1132	0.1188	0.1208	0.1229	0.1262
6	0.0847	0.0891	0.0919	0.0947	0.0947	0.0996	0.1044	0.1078	0.1088	0.1172	0.1178	0.1249	0.1277
7	0.085	0.0858	0.0873	0.0924	0.0924	0.1001	0.1004	0.1037	0.1111	0.116	0.1196	0.1211	0.1244
8	0.0819	0.0847	0.0901	0.0906	0.0906	0.0963	0.1021	0.1068	0.107	0.1142	0.1167	0.1213	0.1244
9	0.0835	0.0847	0.0855	0.0914	0.0914	0.0975	0.1004	0.1019	0.1083	0.1142	0.1188	0.119	0.1231
10	0.0799	0.0812	0.0863	0.0873	0.0873	0.0934	0.0975	0.1044	0.1027	0.1108	0.1152	0.1185	0.1216
11	0.0788	0.0822	0.0809	0.0886	0.0886	0.0945	0.0975	0.0991	0.1039	0.1129	0.1142	0.1155	0.1201
12	0.0778	0.0781	0.0832	0.085	0.085	0.0916	0.094	0.1006	0.1006	0.108	0.1103	0.116	0.1188
13	0.0773	0.0801	0.0788	0.0863	0.0863	0.0911	0.0965	0.096	0.1027	0.1111	0.1124	0.1147	0.1183
14	0.0753	0.0745	0.0814	0.0814	0.0814	0.0901	0.0919	0.0978	0.0993	0.107	0.1083	0.1116	0.1144
15	0.075	0.0768	0.0768	0.0835	0.0835	0.0878	0.0927	0.0929	0.0978	0.1075	0.1096	0.1126	0.1157
16	0.0722	0.0714	0.0768	0.0783	0.0783	0.0876	0.0883	0.0952	0.0968	0.1019	0.106	0.1091	0.1114
17	0.0712	0.0753	0.0753	0.0824	0.0824	0.0852	0.0909	0.0922	0.0947	0.1039	0.106	0.1114	0.1149
18	0.0668	0.0707	0.0735	0.0771	0.0771	0.0852	0.086	0.0919	0.095	0.1004	0.1044	0.1065	0.1101
19	0.0694	0.0709	0.0727	0.0781	0.0781	0.0822	0.0891	0.0899	0.0916	0.1027	0.1021	0.1078	0.1111
20	0.0645	0.0686	0.0701	0.0748	0.0748	0.0827	0.0837	0.0881	0.0919	0.0983	0.1011	0.1016	0.1057
21	0.0671	0.0676	0.0701	0.0748	0.0748	0.0786	0.0855	0.0878	0.0886	0.098	0.0998	0.1055	0.108
22	0.063	0.0663	0.0666	0.0719	0.0719	0.0812	0.0819	0.086	0.0901	0.0968	0.0996	0.1001	0.1032
23	0.0635	0.0645	0.0678	0.0719	0.0719	0.076	0.0819	0.085	0.0858	0.095	0.0955	0.1032	0.106
24	0.0599	0.0625	0.0622	0.0686	0.0686	0.0771	0.0783	0.0817	0.0878	0.0942	0.0968	0.098	0.1011
25	0.0589	0.0591	0.0648	0.0681	0.0681	0.074	0.0788	0.0827	0.0829	0.0911	0.0924	0.0986	0.1016

X/Y(mm)	14	15	16	17	18	19	20	21	22	23	24	25
1	0.1339	0.1362	0.1408	0.1449	0.1485	0.1528	0.1569	0.1603	0.1649	0.169	0.1731	0.1733
2	0.1326	0.137	0.1411	0.1444	0.149	0.1526	0.1549	0.1608	0.1646	0.1682	0.1723	0.1736
3	0.1336	0.1359	0.1395	0.1431	0.1472	0.151	0.1539	0.1577	0.162	0.1667	0.1708	0.1723
4	0.1318	0.1349	0.139	0.1416	0.1469	0.1508	0.1536	0.1585	0.1633	0.1667	0.1702	0.1718
5	0.1313	0.1349	0.1375	0.1423	0.1459	0.15	0.1518	0.1569	0.161	0.1654	0.1687	0.17
6	0.13	0.1339	0.1372	0.1411	0.1454	0.1487	0.1513	0.1567	0.1605	0.1644	0.1679	0.1695
7	0.1285	0.1318	0.1341	0.1398	0.1439	0.1472	0.15	0.1551	0.1587	0.1631	0.1659	0.1679
8	0.128	0.1298	0.1359	0.1385	0.1431	0.1464	0.1492	0.1536	0.1577	0.1608	0.1644	0.1661
9	0.1267	0.1298	0.1334	0.1377	0.1413	0.1449	0.148	0.1526	0.1559	0.1603	0.1641	0.1659
10	0.1254	0.1277	0.1329	0.1364	0.14	0.1449	0.1459	0.1518	0.1559	0.1587	0.1623	0.1636
11	0.1224	0.1285	0.1306	0.1352	0.1388	0.1423	0.1462	0.1492	0.1536	0.1564	0.1605	0.1623
12	0.1229	0.1254	0.1293	0.1331	0.1364	0.1416	0.1444	0.1485	0.1526	0.1564	0.1592	0.1615
13	0.1203	0.1252	0.1285	0.1324	0.1382	0.1413	0.1446	0.1482	0.1518	0.1549	0.1587	0.1605
14	0.1221	0.1234	0.1275	0.1311	0.1354	0.1393	0.1423	0.1462	0.1503	0.1539	0.1574	0.1597
15	0.1178	0.1224	0.1254	0.1293	0.1341	0.137	0.1418	0.1457	0.1495	0.1528	0.1569	0.1582
16	0.1175	0.1193	0.1236	0.1295	0.1321	0.1367	0.14	0.1439	0.1477	0.151	0.1546	0.1567
17	0.1149	0.1203	0.1239	0.1272	0.1321	0.1352	0.1385	0.1428	0.1475	0.1508	0.1546	0.1562
18	0.1155	0.118	0.1206	0.1277	0.1288	0.1341	0.1393	0.1423	0.1459	0.1498	0.1536	0.1559
19	0.1116	0.1167	0.1224	0.1244	0.13	0.1331	0.1367	0.1408	0.1446	0.148	0.1516	0.1536
20	0.1132	0.116	0.118	0.1234	0.1265	0.1298	0.1357	0.1393	0.1434	0.1464	0.151	0.1528
21	0.1106	0.1126	0.1196	0.1211	0.1265	0.1311	0.1331	0.138	0.1428	0.1457	0.1498	0.1513
22	0.1096	0.1144	0.1149	0.1211	0.1252	0.1285	0.1329	0.1364	0.1408	0.1444	0.1485	0.15
23	0.1083	0.1108	0.1162	0.1188	0.1231	0.1277	0.1298	0.1357	0.14	0.1439	0.1469	0.1492
24	0.1047	0.1108	0.1108	0.1178	0.1213	0.1252	0.1308	0.1339	0.1375	0.1416	0.1452	0.1469
25	0.1055	0.107	0.1132	0.1157	0.1201	0.1242	0.1272	0.1313	0.1359	0.1395	0.1431	0.1452

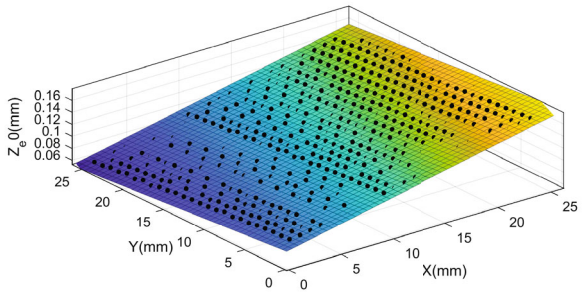

Fig. 10. Fitting plane of the point cloud.

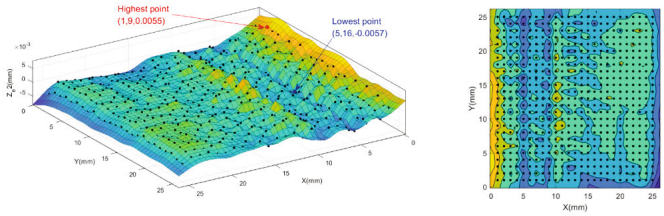

(a) Fitting surface (b) Contour map

Fig. 11. Information on the surface of the cooled detector.

distance between the initial data and the fitting plane is calculated. The fitting plane of the detector is as shown in Fig. 10, the R^2 of the fitting plane is 0.9962, and the adjusted R^2 is 0.9962.

The equation of the fitting plane from the array point is

$$Z\_e1 = 0.08567 + 0.003698 \cdot X - 0.001263 \cdot Y \qquad (3)$$

And the deviation between the collection point and the fitting plane is

$$Z\_e2 = Z\_e0 - Z\_e1 \qquad (4)$$

After re-fitting the revised data, we obtain the fitting surface and the contour map are shown in Fig. 11. After calculation, the RMS value of the cooled detector is 0.0017 mm, and the PV value is 0.0112 mm. The highest and the lowest points appear at (1, 9, 0.0055) and (5, 16, −0.0057), respectively.

3. Flatness Changes Before and After Cooling

The flatness of the Princeton Instruments Quad-RO 4320 camera under uncooled and cooled conditions was measured. The conclusion can be drawn from the above results that the detector has a good flatness. Although the shape of the detector's surface changes after cooling, the change tends to be positive, and in the four corners of the detector, the changes are especially large, as shown in Fig. 12, which shows that the detector of the camera has very good ability to maintain flatness.

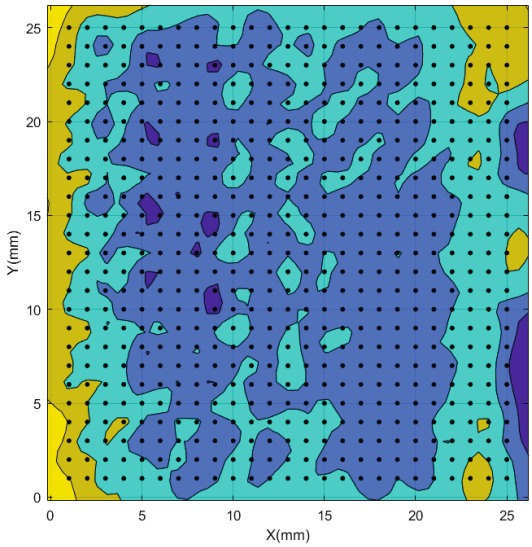

Fig. 12. Contour map after cooling.

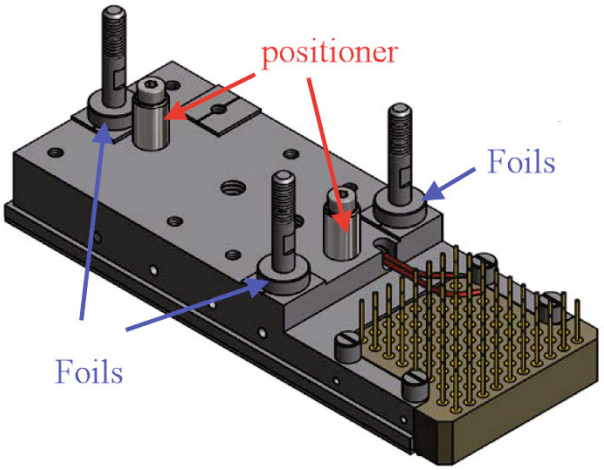

Fig. 13. Mosaic detector CIS113 from e2v.

V. FLATNESS MEASUREMENT FOR MOSAIC DETECTORS

1. Overview of Mosaic Detectors

Measuring a mosaic array of detectors is a complex process, for which the cooling, assembly, and packaging of the detectors needs to be considered. This paper only describes the flatness measurement and data processing of mosaic detectors at room temperature. Shown in Fig. 13 is the back view of the e2v CIS 113 mosaic detector from England. Two high-precision positioning columns can realize precise positioning of the detector on the basilar plate, and three adjustable gaskets are used to adjust the relative height and tilt between the detectors.

The process of mosaic detector integration is as fol-

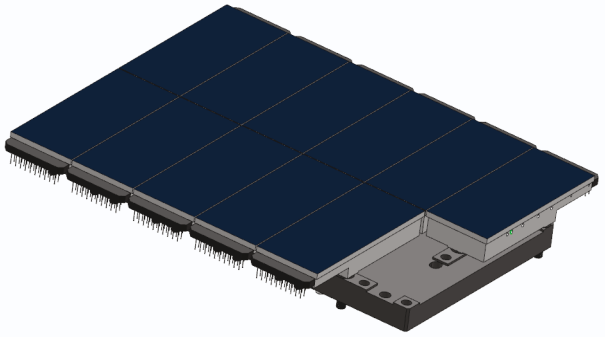

Fig. 14. Model for the mosaic dummy.

lows:

a) Measure the relative height between the sensitive surface of each detector and the installation reference.
b) Measure the flatness of the mounting surface of the detector-mounting basilar plate.
c) Allocate the installation position according to the height deviation of the detector and the flatness of the installation base plate.
d) Calculate the thickness of the foils needed for the coplanar mosaic detector.
e) Place the corresponding foils on each installation base surface of the detector and pre-tighten the screw bolt preliminarily, and then use a standard thickness gauge to ensure the detector interval is consistent.
f) Use a torque wrench to tighten the mounting nuts to fix all detectors with the same torque.
g) Use the measurement platform to measure the flatness of the mosaic detectors, calculate the RMS and PV value of the flatness, remove the detector with the largest deviation, and adjust the foils; repeat the process until the requirements are met.
h) Put the mosaic detectors in the vacuum experimental chamber and measure the flatness of the cooled focal plane to ensure that the requirements are met.
i) Install the mosaic detector in the final dewar chamber, measure the relative position between the focal plane and the dewar installation reference plane, and adjust the installation position of the splicing detector to ensure that the tilt and the piston meet the optical imaging requirements.

2. Flatness Measurement of Mosaic Detectors

To prevent pollution and damage to the detectors we used, a mosaic dummy model for the flatness measurement. As shown in Fig. 14, a 2 × 6 mosaic focal plane was

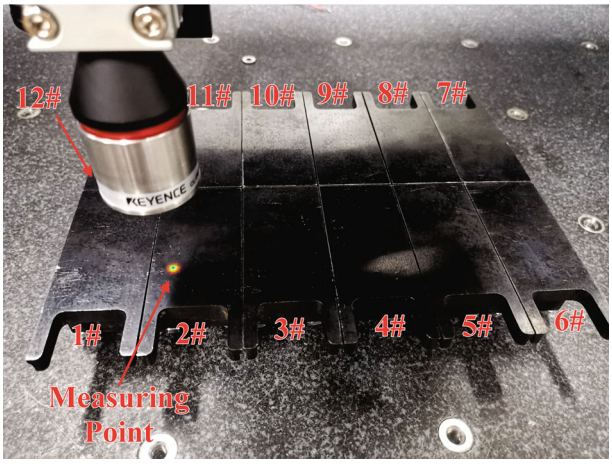

Fig. 15. Measurement of the mosaic detectors.

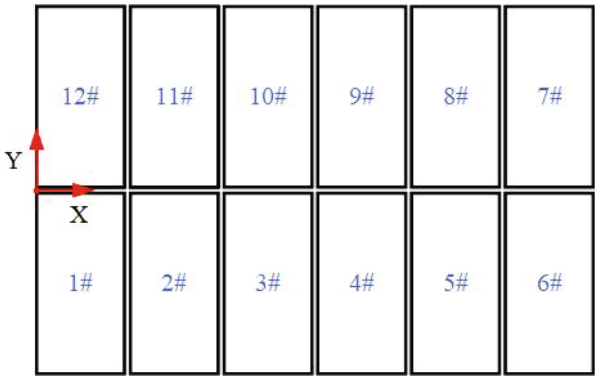

Fig. 16. Coordinates and number of the mosaic focal plane.

designed using the e2v CIS113 model. The mosaic model is made of metal. The surface of the mosaic dummy model to be measured is ground to a flatness of 10 μm, after which the preliminary installation and adjustment are carried out. After the installation and adjustment, the surfaces of the mosaic detectors are measured, as shown in Fig. 15.

Before the measurement, a coordinate system was established for the mosaic detector model, and the dummy detectors were numbered, as shown in Fig. 16. After completing the value of each detector array point, we carried out preliminary data processing for the flatness of the mosaic focal plane. The overall tilt of the 12# detector relative to the other errors is large, and the deviation of the other detectors has been submerged. During the experiment, comparing the experimental results with those obtained using the mosaic detector model, we found that, indeed, the position deviation of detector 12# was large.

After modifying and reinstalling the foils for detector 12#, and then re-measuring the array points of the focal plane, we obtained the results are shown in Fig. 17. As can be seen from the figure, an obvious tilt caused by the overall placement of the mosaic detectors can be seen, so reinstalling and adjusting the foils to fix this tilt is neces-

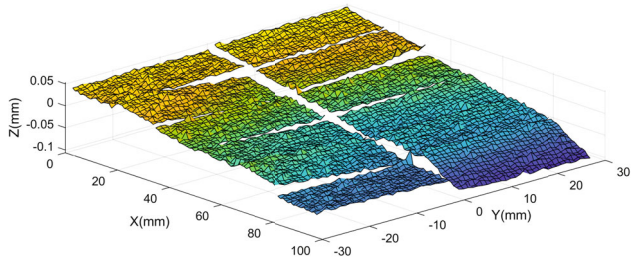

Fig. 17. Array points in the focal plane of the mosaic.

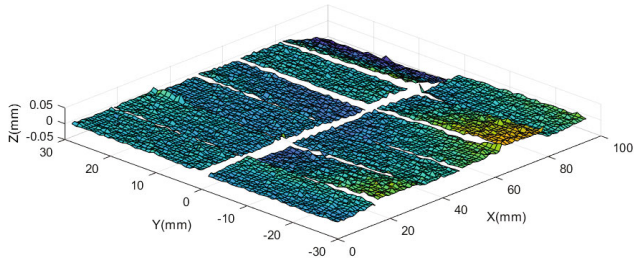

Fig. 18. Array points of the focal plane of the mosaic after correction.

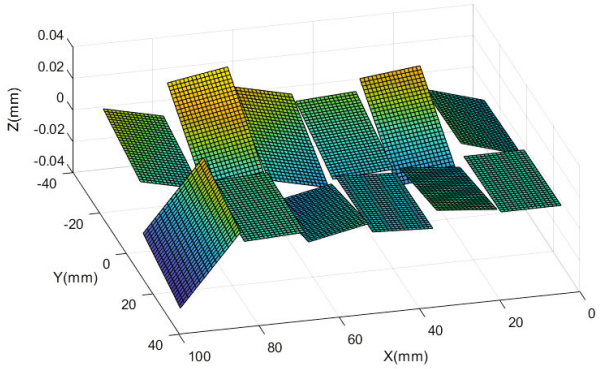

Fig. 19. Relative position between detectors.

sary. This tilt also occurs between the mosaic focal plane and the dewar installation datum, and this error should be corrected during component installation. The equation of the overall inclined plane is fitted and calculated, and subsequently, all array points are corrected to obtain the flatness of the mosaic detector model, as shown in Fig. 18. The flatness of the mosaic focal plane is mainly affected by the flatness of a single detector and relative positions of the detectors. After receiving the detectors, we can only adjust the relative positions in the splicing process. As shown in Fig. 19, the relative positions of the detectors are mainly height and angle deviation. After calculation, the initial RMS setting of the splicing detector model is 0.009 mm, and the PV value is 0.0808 mm, as shown in Fig. 20. In this paper, only the flatness measurement and data processing in the development process of a splicing detector were studied.

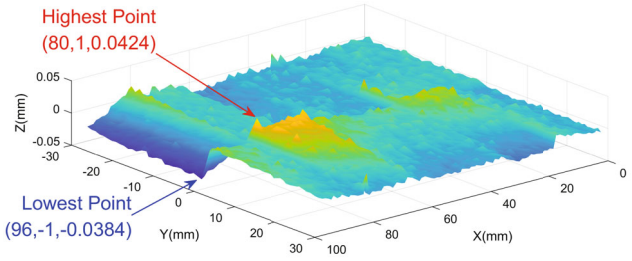

Fig. 20. Flatness of the focal plane of the mosaic.

VI. CONCLUSION

In this paper, the flatness measurement method of the mosaic focal plane in a large-aperture, wide field-of-view telescope is studied. The method of using a coaxial multispectral laser displacement meter and a high-precision double-drive gantry platform to measure the flatness of a single detector and dummy mosaic detectors is proposed, and a detailed data analysis is carried out. Comparisons showed that the RMS and PV experimental results can reflect the true shape characteristics of the detectors, which shows that this measurement method can be used in the development of wide field of view mosaic detectors. However, the amount of data in this measurement is huge. In the experimental process, data are recorded first, after which the data processed. The timeliness is poor. In the follow-up research, the software needed for automatic measurement and data analysis will be designed.

ACKNOWLEDGMENTS

The authors would like to thank Jian-Li Wang and Tao Chen for their helpful discussions and valuable technological help. This work is supported by the National Key Technologies R&D Program of China for space debris exploration.

REFERENCES

[1] A. P. Rasmussena *et al.*, Proc. SPIE **6273**, 62732U (2006).
[2] B. Atwood *et al.*, Proc. SPIE **8446**, 84466G (2012).
[3] Y. Kamata *et al.*, Proc. SPIE **8453**, 84531X (2012).
[4] M. Antonik *et al.*, Proc. SPIE **7433**, 74330M (2009).
[5] P. S. Salter and M. J. Booth, Light Sci. Appl. **8**, 110 (2019).
[6] K. Wang *et al.*, Opt. Precis. Eng. **28**, 39 (2020).
[7] Y-K. Li, Y-L. Wang and H-H. Huang, Opt. Precis. Eng. **27**, 2659 (2019).